Transient Simulation and Control strategy of Supercritical CO_2 Solar Thermal Power Generation System

Feng Hu[1,2,3,4], Zhifeng Wang[1,2,3,4*]

[1] Key Laboratory of Solar Thermal Energy and Photovoltaic Systems, Beijing (China)

[2] Institute of Electrical Engineering, Beijing (China)

[3] University of Chinese Academy of Sciences, Beijing (China)

[4] Beijing Engineering Research Center of Solar Thermal Power, Beijing (China)

Abstract

In order to mitigate climate change and promote energy revolution, it is imperative to develop new energy technology of supercritical carbon dioxide (sCO_2) solar thermal power generation. By studying the basic scientific problems of the integration of the sCO_2 Breton cycle with the solar tower (SPT) station, it will contribute to the realization of the zero-carbon scenario. By establishing the dynamic simulation model of the integrated system, the key parameters of the system are determined, and the transient simulation and control strategy are studied. The results show that the efficiency of the system decreases by 3.1% at 75% load operation and 9.5% at 50% load operation compared with 100% load operation. Compared with conventional inventory control, the power generation of the system on the summer solstice and winter solstice after adopting extremum-seeking control increased by 2.06% and 1.61%, after adopting differential evolution control increased by 2.13% and 1.69%. While, when the DNI exceeds 600W/m^2, extremum-seeking control shows greater advantage compared with differential evolution control. At last, some suggestions on promoting clean energy technology innovation are put forward.

Keywords: Climate change; Supercritical carbon dioxide; Concentrated solar power; Simulation; Control

1. Introduction

Since the nineties of the 20th century, the change of global climate system, which is mainly characterized by climate warming, has become the most severe environmental challenge faced by mankind. A warming climate will threaten food, water, ecosystems, extrmme weather events, risk of abrupt and major irreversible changes and more. As shown in Fig. 1, in order to cope with climate change, from the first World Climate Conference held in Geneva in 1979 to the upcoming COP26 in 2021, countries around the world have formulated relevant policies and taken effective measures. On the occasion of the fifth anniversary of the Signing of the Paris Agreement, China has announced to the world its national goal of achieving carbon peak by 2030 and carbon neutral by 2060. At that time, renewable energy will play a major role and become the main body of energy increment (Chen Y, 2021). Energy technological innovation is a key direction for carbon neutrality in the future. Promoting global technological change through innovation is likely to be a game changer for international climate change action and can reduce the cost of climate change mitigation and adaptation. Concentrated Solar Power (CSP) is considered as one of the most promising renewable energy generation methods due to its relatively mature technology and low impact on the Power grid, which can generate electricity continuously for 24 hours (Wang Z, 2019). As a new energy technology, sCO_2 solar thermal generation technology can not only rationally utilize the greenhouse gas carbon dioxide in the air, but also improve the efficiency of clean energy generation (He Y et al, 2020), its optimized design and dynamic simulation will make corresponding contributions to promoting the energy revolution and mitigating climate change.

doi:10.18086/swc.2021.19.01 Available at http://proceedings.ises.org

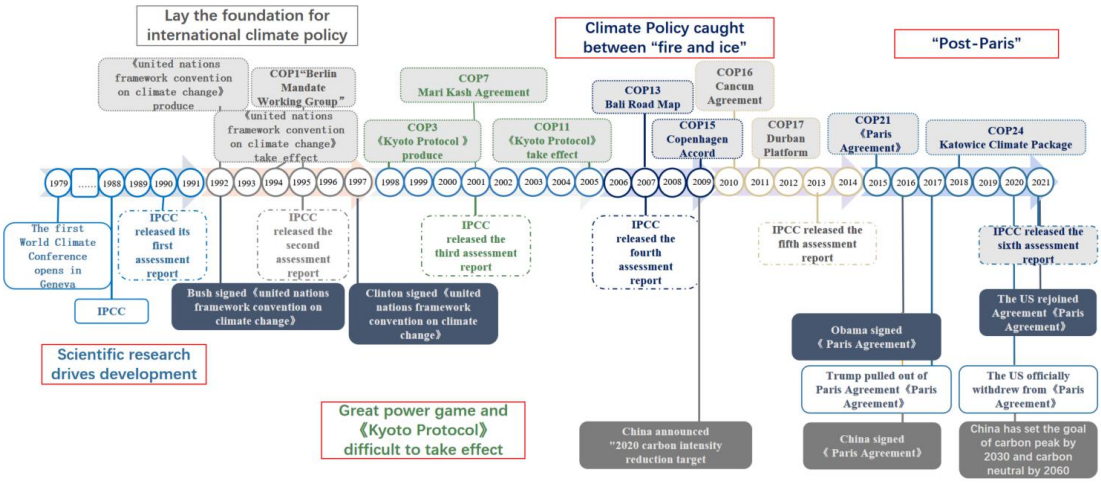

Fig. 1: Major international climate governance events

In order to solve the basic problem of the sCO_2 Brayton cycle integrated with SPT station which used solid particle solar receiver (SPSR), it is necessary to carry out optimization design and dynamic simulation analysis of the integrated system. However, most studies have been focusing on the analysis of steady state operations in the integration between the solar heating block and the sCO_2 cycle, respectively (Al-Sulaiman et al, 2015; Cheang, 2015; Daabo, 2017). There is relatively rare literature works have addressed the controllability problems of it. Singh et al. (2013) conducted dynamic and process control analyses for a solar-assisted Brayton cycle utilizing a simple layout. Minh et al. (2018) investigate the dynamic behavior and control for a direct-heating solar-assisted recompression cycle. Control strategies are developed for the Brayton cycle to reduce the effect of perturbations in the net solar power and sustain stable operation. However, their studies were all based on the control of sCO_2 inventory in the sCO_2 cycle block, without controlling the inventory of working medium in the solar heating block at the same time. Based on the previous work, the dynamic simulation model of the integrated system is established, and the performance of the system is compared and analyzed by using different control strategies. Aiming at the first solar thermal power generation system pre-built in China, which integrates SPSR and sCO_2 Brayton cycle, corresponding control logic of two typical sunsets in summer solstice and winter solstice were preliminarily analyzed, aiming at laying a foundation for the research of predictive control. By establishing models to calculate the effects of particle size, circulating pressure ratio, turbine and compressor inlet temperature, and regenerator end error on the system performance, the parameters of the integrated system were optimized. By combining the non-dominant sorting genetic algorithm with the printed circuit heat exchanger (PCHE) substitute model calculated by the quasi-two-dimensional heat transfer model, the multi-objective optimization of the PCHE thermo-hydraulic performance was realized, and the Pareto optimal solution set of the temperature rise and pressure drop of the target variables and the corresponding dimensional variable variation characteristics were obtained. By using the extremum-seeking control and differential evolution control strategy, the dynamic characteristics of the system are simulated.

2. Optimization Design

As shown in Fig. 2, aiming at the first sCO_2 solar thermal power plant pre-built in China, which integrates quartz tube bundle SPSR, fluidized bed particle/ sCO_2 heat exchanger, PCHE and turbine/ compressor.

During the time with sunlight, the heliostat field reflects and concentrates the sunlight to the SPSR on the top of the tower. The particles, which flow from the cold tank, is heated to a high temperature in the SPSR, and then flow into the hot tank. The mass flow rate of particles in the SPSR is adjusted in accordance with the varying solar irradiation to maintain a constant temperature of particles at the outlet of the SPSR. Part of the particles in the hot tank pass through the heat exchanger to transfer heat to the sCO_2 Brayton cycle, and then return to the cold tank. During the time lacking sunlight, the particles in the hot tank discharge and heat CO_2 in the heat exchanger, and finally is stored in the cold tank. In the sCO_2 Brayton cycle, the low- pressure CO_2 at state 1 is compressed to the high-pressure state 2. Then the high-pressure CO_2 is heated to state 3 in the recuperator by the low-pressure CO_2 which undergoes the process from state 5 to state 6, and subsequently heated to state 4 in the

heater by the particles from the hot tank. The high-temperature and high-pressure CO_2 at state 4 expands in the turbine to state 5, then the exhausted CO_2 undergoes the process from state 5 to state 6 in the recuperator, releasing heat to heat the high-pressure CO_2 at state 2 up to state 3. Finally, the CO_2 at state 6 exits from the recuperator and is cooled down to state 1 in the cooler.

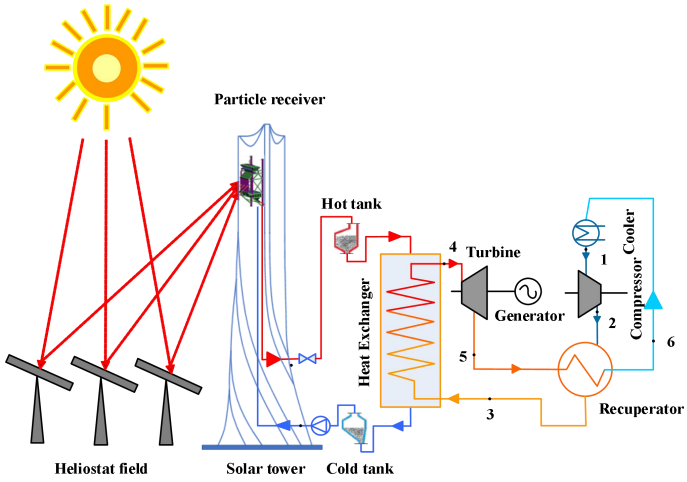

Fig. 2: System schematic diagram

Tab. 1: Design parameters of Badaling sCO_2 Concentrated Solar Power Plant (Wang Z, 2019; Nie F, 2020).

Symbol	Quantity	Value
Φ	Location	40.4°N 115.9°E
N_{hel}	Heliostat Number	100
A_{hel}	Each heliostat size	100 m^2
ρ_{hel}	Mirror reflectance	0.9
η_{hel}	Optical Efficiency of Field	66.6%
H_t	Tower height	92 m
$N_{R,t}$	Quartz tube number of SPSR	20
$L_{R,t}$	Length of each tube	2.5 m
$D_{R,out}$	Outer diameter of quartz tube	110 mm
$D_{R,in}$	Inner diameter of quartz tube	100 mm
ρ_p	Density of particle	1750 $kg \cdot m^{-3}$
D_p	Mean particle diameter	718 μm
$C_{p,p}$	Specific heat of particle	$(1.76\times10^{-6}T^3-3.54\times10^{-3}T^2+2.7T+12.7)$ J/(kg·K)
k_p	Thermal conductivity of particle	(6.18×10-4T+0.0222) W/(m·K)
α_p	Solar weighted absorptance	0.94
ε_p	Total, normal emittance	0.85
M_T	Mass of hot/cold tank	25 t
M_p	Mass of particles stored in the tank	10 t
q_L	Heat loss power of hot/cold tank	600 W/ m^2
T_h	Temperature of hot tank	1073 K
T_c	Temperature of cold tank	823 K

S_{HX}	Shell size of HX	4.5m×2m×4.5m
$N_{HX,t}$	Tube number of HX	28
$L_{HX,t}$	Total length of a single tube	28.8 m
$\rho_{HX,t}$	Density of HX tube	9000 kg·m^{-3}
$D_{HX,in}$	Inner diameter of HX tube	36 mm
$D_{HX,ex}$	External diameter of HX tube	45 mm
V_{air}	Air volume in the fluidized bed	3820 N·m^3/h
$m_{HX,p}$	Mass flow rate of particle in the HX	30 t/h
$m_{HX,CO2}$	Mass flow rate of sCO_2 in the HX	16.6 t/h
$P_{HX,w}$	Pressure of fluidized wind	54.5 kPa
$P_{HX,p}$	Pressure of particle side	0.101 MPa
$P_{HX,CO2}$	Pressure of sCO_2 side	15.7 MPa
$T_{t,in}$	Turbine inlet temperature	823 K
$P_{t,in}$	Turbine inlet pressure	14.1 MPa
$\eta_{k,t}$	Pressure ratio of turbine	1.602
$\eta_{t,is}$	Turbine isentropic efficiency	74%
s_t	Speed of turbine	20000 rpm
W_t	Shaft power of turbine	528 kW
$T_{c,in}$	Compressor inlet temperature	308 K
$P_{c,in}$	Compressor inlet pressure	8.2 MPa
$\eta_{k,c}$	Pressure ratio of compressor	1.829
$\eta_{c,is}$	Compressor isentropic efficiency	73.5%
s_c	Speed of compressor	28000 rpm
W_c	Shaft power of compressor	170 kW
η_g	Generator efficiency	97%
η_m	Motor efficiency	90%
S_{re}	Size of recuperator	903mm×314mm×450mm
$T_{r,in,h}$	Inlet temperature of hot side	789.6 K
$T_{r,out,h}$	Outlet temperature of hot side	342.8 K
$T_{r,in,c}$	Inlet temperature of cold side	332.8 K
$T_{r,out,c}$	Outlet temperature of cold side	691.74 K
S_c	Size of cooler	900mm×290mm×450mm
$T_{c,in,h}$	Inlet temperature of hot side	362.8 K
$T_{c,out,h}$	Outlet temperature of hot side	308 K
$T_{c,in,c}$	Inlet temperature of cold side	298 K
$T_{c,out,c}$	Outlet temperature of cold side	311 K
ΔP_{PCHE}	Pressure drop of PCHE	0.3 MPa
$m_{cyc,CO2}$	Mass flow rate of sCO_2 in the turbine /compressor/PCHE	36 t/h

To analyze the system, the mathematical model of relevant components is established based on the law of conservation of energy, using the mult-section lumped parameter method. And each sub-model is verified.

For Heliostat field, the energy delivered from it can be calculated as:

$$Q_{rec} = Q_{solar} \cdot \eta_{hel} = DNI \cdot A_{hel} \cdot \eta_{hel} \quad \text{(eq.1)}$$

Where Q_{rec} is the effective heat gain of the receiver, W; Q_{solar} is the incident solar energy, W.

For solid particles in the SPSR, the microelement segment ΔL is taken as the modeling object， the energy conservation can be calculated as:

$$c_p \rho_p V_p \frac{dT_p}{dt} = (c_{p,\text{in}} m_{p,in} T_{p,in} - c_{f,\text{out}} m_{p,out} T_{out}) + (q_{rec,p} - q_{rad,p\text{-}qt} - q_{conv,p\text{-}qt}) \cdot \Delta L \quad \text{(eq.2)}$$

Where c_p is the specific heat capacity of particles, J/(kg·K); ρ_p is the density of particles, kg·m^{-3}; V_p is the volume of particles, m^3·kg^{-1}; m_p is the mass flow rate of particles, kg·s^{-1}.

The heat flux absorbed by solid particles is:

$$q_{rec,p} = \tau_{qt} \alpha_p q_{rec} \quad \text{(eq.3)}$$

Where c_p is the specific heat capacity of particles, J/(kg·K); τ_{qt} is the transmittance of quartz glass tube.

The radiant heat flow between the solid particles and the inner wall of the quartz tube is:

$$q_{rad,p\text{-}qt} = \frac{\sigma \pi D_{in} \left(T_p^4 - T_{qt}^4\right)}{1/\varepsilon_p + 1/\varepsilon_{qt} - 1} \quad \text{(eq.4)}$$

Where σ is the Stefan Boltzmann constant; T_p and T_{qt} are average temperature of particles and quartz glass tube, K; ε_p and ε_{qt} are the emittance of particles and quartz glass tube.

The convective heat flow between the solid particles and the inner wall of the quartz tube is:

$$q_{conv,p-qt} = h_{p,qt} \pi D_{in} \left(T_p - T_{qt}\right) \quad \text{(eq.5)}$$

Where $h_{p,qt}$ is the heat transfer coefficient between particles and quartz tube, W m^{-2} K^{-1}.

The convective heat transfer correlation formula is calculated using the research method of Albrecht and Ho (2018) for the convective heat transfer between solid particles and the wall surface in the horizontal push flow in the rectangular flow passage. The solid particles in the flow passage are regarded as the continuous medium with constant flow distribution:

$$h_{p,qt} = \frac{\lambda_{eff}}{D} \overline{Nu_q} = \frac{\lambda_{eff}}{D} \left[\left(2 \times \frac{0.886}{\sqrt{Gz^{-1}}} \right)^{12/5} + 12^{12/5} \right]^{5/12} \quad \text{(eq.6)}$$

Where λ_{eff} is the Thermal conductivity of particles, W m^{-1} K^{-1}; Nu_q and Gz^{-1} are dimensionless number.

For TES, the energy conservation can be calculated as:

$$\frac{d\left(M_{hot,\tan k} \cdot c_p \cdot T_{p,hot,\tan k}\right)}{dt} = m_{rec} \cdot c_p \cdot T_{p,hot,\tan k} - m_{HX} \cdot c_p \cdot T_{p,HX,out} - Q_{loss,\text{hot},\tan k} \quad \text{(eq.7)}$$

$$\frac{d\left(M_{cold,\tan k} \cdot c_p \cdot T_{p,cold,\tan k}\right)}{dt} = m_{HX} \cdot c_p \cdot T_{p,HX,out} - m_{rec} \cdot c_p \cdot T_{p,cold,\tan k} - Q_{loss,\text{cold},\tan k} \quad \text{(eq.8)}$$

Where $M_{hot,tank}$ and $M_{cold,tank}$ are quality of high temperature tank and low temperature tank, kg; m_{HX} and m_{rec} are mass flow rate of heat exchanger and receiver, kg s^{-1}.

For the gas-solid mixing side, the tube and sCO_2 side of the HX, the energy conservation can be calculated as:

$$\left(c_{p,p} \rho_p V_p + c_{p,g} \rho_g V_g\right) \frac{dT_m}{dt} = \left(-q_{rand,m-t} - q_{conv,m-t}\right) \cdot \Delta L + \left(c_{p,p} m_p + c_{p,g} m_g\right)\left(T_{\text{m},in} - T_{m,out}\right) \quad \text{(eq.9)}$$

$$c_{p,t}\rho_t V_t \frac{dT_t}{dt} = \left(q_{rand,m-t} + q_{conv,m-t} - q_{conv,t-CO_2}\right)\cdot \Delta L \quad \text{(eq.10)}$$

$$c_{p,CO_2}\rho_{CO_2} V_{CO_2} \frac{dT_{CO_2}}{dt} = q_{conv,t-co2}\cdot \Delta L + c_{p,CO_2,in} m_{CO_2,in} T_{CO_2,in} - c_{p,CO_2,out} m_{CO_2,out} T_{CO_2,\,out} \quad \text{(eq.11)}$$

Where $c_{p,p}$, $c_{p,t}$ and c_{p,co_2} are specific heat capacity of particles, tube and carbon dioxide, J/(kg·K); ρ_p, ρ_t and ρ_{co_2} are density of particles, tube and CO_2, kg·m^{-3}; V_p, V_t and V_{co_2} are volume of particles tube and CO_2, m^3·kg^{-1}; m_p, m_g and m_{co_2} are the mass flow rate of particles, gas and CO_2, kg·s^{-1}.

Radiant heat flux is:

$$q_{rand,m-t} = \frac{\sigma\pi D_{out}\left(T_m^4 - T_t^4\right)}{1/\varepsilon_p + 1/\varepsilon_t - 1} \quad \text{(eq.12)}$$

Where T_m and T_t are average temperature of fluidized particles and heat exchanger tube, K.

Convective heat flux is:

$$q_{conv,m-t} = h_{conv,m-t}\pi D_{out}\left(T_m - T_t\right) \quad \text{(eq.13)}$$

Where $h_{conv,m-t}$ is the heat transfer coefficient between fluidized particles and heat exchanger tube, W m^{-2} K^{-1}.

The convective heat flux between the heat exchange tube and the CO_2 in the tube is:

$$q_{conv,t-CO_2} = h_{conv,t-CO_2}\pi D_{in}\left(T_t - T_{CO_2}\right) \quad \text{(eq.14)}$$

Where $h_{conv,t-co2}$ is the heat transfer coefficient between heat exchanger tube and CO_2, W m^{-2} K^{-1}.

The heat-transfer coefficient from the correlations of Borodulya (1991) and Gnielinski (1976):

$$h_{conv,m-t} = Nu_p \frac{\lambda_g}{d_p} = \left(0.74 Ar^{0.1}\left(\frac{\rho_p}{\rho_g}\right)^{0.14}\left(\frac{Cp_p}{Cp_g}\right)^{0.14}\left(1-\varepsilon\right)^{2/3} + 0.46\,\mathrm{Re}\,\mathrm{Pr}\frac{\left(1-\varepsilon\right)^{2/3}}{\varepsilon}\right)\frac{\lambda_g}{d_p} \quad \text{(eq.15)}$$

$$h_{conv,t-CO_2} = Nu_{CO_2}\frac{\lambda_{CO_2}}{d_{hd}} = 0.0214\left(\mathrm{Re}_{CO_2}^{0.8} - 100\right)\mathrm{Pr}_{CO_2}^{0.4}\left[1+\left(\frac{D_{in}}{L}\right)^{2/3}\right]\left(\frac{T_{CO_2}}{T_t}\right)^{0.48}\frac{\lambda_{CO_2}}{D_{in}} \quad \text{(eq.16)}$$

For PCHE, equal heat flow method was used in the model. When the total heat transfer is fixed, the total heat transfer is divided into N parts.

$$c_{Ph,j} m_h (T_{hj,i} - T_{hj,o}) = c_{Pc,j} m_c (T_{cj,o} - T_{cj,i}) = \frac{Q_{tot}}{N} = U_j A_j \Delta T_j \quad \text{(eq.17)}$$

In the sinusoidal flow channel of the recuperator, the correlation equation between heat transfer and resistance of sCO_2 are:

$Nu = 0.246Re^{0.6513}Pr^{1.5647}$ (eq.18)

$f = 5.5119Re^{-0.35}$ (eq.19)

On the water side of the precooler, the correlation equation of heat transfer and resistance are:

$Nu = 0.062063Re^{0.765}$ (eq.20)

$f = 16.79364Re^{-0.368}$ (eq.21)

On the sCO_2 side of the precooler, the correlation equation of heat transfer and resistance are:

$Nu = 0.0506Re^{0.8356}$ (eq.22)

$f = 524.0253Re^{-0.6743}$ (eq.23)

For the turbine and compressor, the model is referenced from SNL (Conboy, 2012; Wright, 2011):

$$m_{co_2} = C_T A_{eff}\rho_{T,out} \quad , \quad C_T = \sqrt{2\Delta h_{T,is}} \quad \text{(eq.24)}$$

$$\phi^* = \frac{m_{co_2}}{\rho U_c D_c^2}\left(\frac{N}{N_{design}}\right)^{1/5}, \quad \psi_i^* = \frac{\Delta h_i}{U_c^2}\left(\frac{N_{design}}{N}\right)^{(20\phi^*)^3}, \quad \eta^* = \eta\left(\frac{N_{design}}{N}\right)^{(20\phi^*)^3} \qquad \text{(eq.25)}$$

For the integrated system, the sCO_2 cycle efficiency and net power generation efficiency are respectively：

$$\eta_{sCO_2} = \frac{\left(h_{T_{in}} - h_{T_{out}}\right)\cdot\eta_G - \left(h_{C_{out}} - h_{C_{in}}\right)/\eta_{motor}}{h_{T_{in}} - h_{HX_{in}}} \qquad \text{(eq.26)}$$

$$\eta_{solar-el} = \frac{\sum_t P_{el,solar}\cdot\Delta t}{\left(\sum_t DNI\cdot A_{hel}\cdot\Delta t\right)\cdot\left(\frac{\sum_t Q_{solar-cycle}\cdot\Delta t}{\sum_t Q_{solar-TES}\cdot\Delta t}\right)} \qquad \text{(eq.27)}$$

Where $h_{T_{in}}$ and $h_{T_{out}}$ are enthalpy of turbine inlet and outlet, $J\cdot kg^{-1}$; $h_{C_{in}}$ and $h_{C_{out}}$ are enthalpy of compressor inlet and outlet, $J\cdot kg^{-1}$; $h_{HX_{in}}$ is enthalpy of heat exchanger inlet, $J\cdot kg^{-1}$; η_G and η_{motor} are efficiency of generator and motor; $P_{el,solar}$ the net solar power generation, W; $Q_{solar-cycle}$ and $Q_{solar-TES}$ are solar energy input into the power cycle and transferred to the heat storage tank, W.

After clarifying the operating mechanism of the system, the key parameters in the system, such as particle size, circulating pressure ratio, turbine and compressor inlet temperature, and regenerator end error, are optimized and designed.

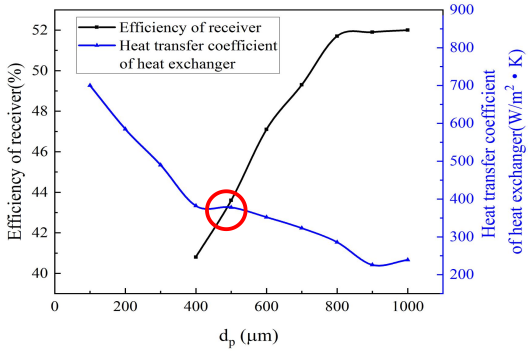

Fig. 3: Particle size selection

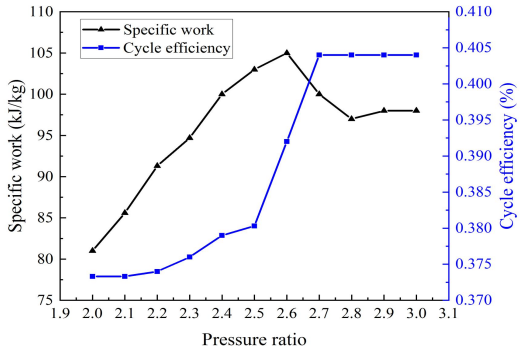

Fig. 4: Pressure ratio selection

As the heat medium, particles directly affect the efficiency of solar receiver and the performance of heat exchanger. As shown in Fig. 3, when the particle size is 0.5mm, simultaneously guarantee efficiency of receiver and coefficient of heat transfer of heat exchanger.

Cycle pressure ratio directly affects turbine power output and compression power consumption. As shown in Fig. 4, when the cycle pressure ratio greater than 2.6, with the increase of it, compression power consumption rises above the turbine output power increase amplitude. The main reason is: at this time the compressor inlet parameters near the CO_2 critical point, the CO_2 density are greatly influenced by pressure and temperature, the small changes of the pressure can lead to large fluctuations in the density, thus bring larger compression power consumption change. When the pressure ratio is 2.6, simultaneously guarantee specific work and cycle efficiency.

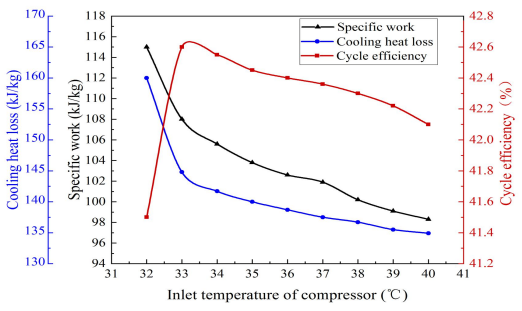

Fig. 5: Compressor inlet temperature selection

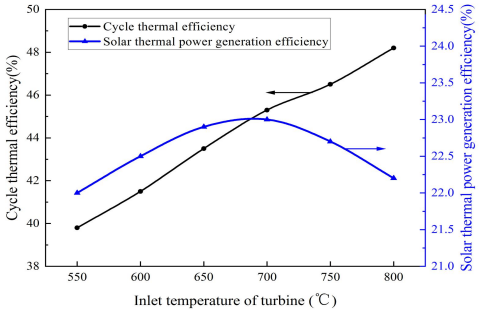

Fig. 6: Turbine inlet temperature selection

Compressor inlet temperature will directly affect the compression and cooling process, so it is an important parameter in the sCO_2-CSP system. As shown in Fig. 5, In the simple regenerative cycle, with the increase of the compressor inlet temperature, compression work consumption rise cycle specific work is reduced, which cause a decline in cycle efficiency. However, compressor inlet temperature increases, the heat release of sCO_2 in cooler decreases, loop heat loss is reduced, the cycle heat loss reduction is beneficial to promote the efficiency of circulation. Therefore, the cycle efficiency of simple heat recovery cycle increases first and then decreases under the dual influence of cycle specific work and cycle heat loss. When the compressor inlet temperature is 33℃, cycle thermal efficiency is the highest.

Turbine inlet temperature is also one of the important parameters affecting system performance. As shown in Fig. 6, with the increase of turbine inlet temperature, the solar heat collection temperature increases, and the heat loss of the solar receiver also increases, resulting in the decrease of receiver efficiency, and then the decrease of solar heat collection efficiency. Due to the dual influence of cycle thermal efficiency and solar heat collection efficiency, there exists an optimal turbine inlet temperature to make solar power generation efficiency reach the maximum value. When the turbine inlet temperature is 650-700 ℃, simultaneously guarantee cycle efficiency and power generation efficiency.

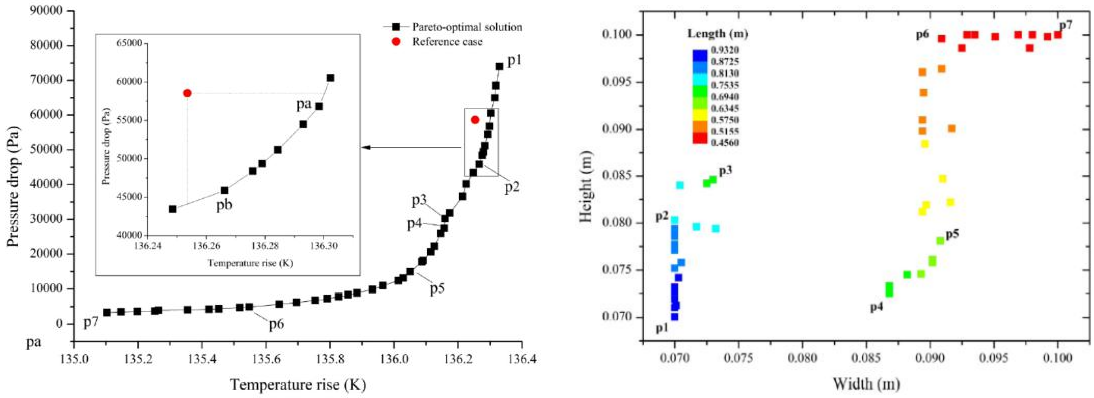

(a) Pareto optimal solution obtained by optimization **(b) Size corresponding to the Pareto optimal solution**

Fig. 7: The optimization design results of PCHE

Besides, in order to establish the relationship between the design variables and the target variables, the multi-objective optimization method adopts NSGA-II. Firstly, a group of random groups is generated in the design variable space. Then, each individual in the group was evaluated with the adaptive equation, that is, the established substitute equation; Then, the individuals in the group were ranked based on the non-dominant ranking method, and the sub-groups were generated by binary league selection, crossover and mutation operations, with the probability of crossover and mutation being 0.9 and 0.1, respectively. The original group and subgroups were combined into a new group, the new group was sorted by non-dominant order, and each individual was given a crowding factor parameter. The next generation's group will consist of well-adjusted individuals from the previous generation's group. Such iterative calculation, until the maximum number of iterations, the final result will be Pareto optimal solution, as shown in Fig. 7. To obtain the optimal Pareto solution and its corresponding size distribution, the pressure drop of PCHE after optimization can be reduced compared with the reference heat exchanger26%, or a 0.4% increase in the temperature of the cold side fluid.

3. Dynamic Simulation

The transient simulation was done on TRNSYS. While the thermodynamic and transport properties of sCO_2 are determined with the assistance of NIST database embedded in TRNSYS.

Due to the intermittent nature of solar irradiation, it is necessary to study the variation of the net output power and different efficiency of the system on typical days under different meteorological conditions with time. Based on the study of simulation system, the dynamic variation rule of thermodynamic performance of typical day system on spring equinox and autumn equinox is analyzed. The results show that with the increase of solar radiation intensity, the heat collection efficiency and the total amount of solar heat collection increase, and the system output work, thermal cycle efficiency and solar net power generation efficiency also increase. This is because when the heat collection efficiency and the total amount of solar heat collection increase, in order to ensure that the parameters of

each node of the system are stable around the design parameters, the flow of the working medium of the thermal circulation increases, and the efficiency of the compressor and turbine is also raised to near its rated efficiency, so that more net output work can be obtained. As shown in Fig. 8, the net output power of the system in a typical day can reach 200kW, and then the thermodynamic cycle efficiency and solar net power generation efficiency of the system reach their maximum 41.35% and 23.02%, respectively.

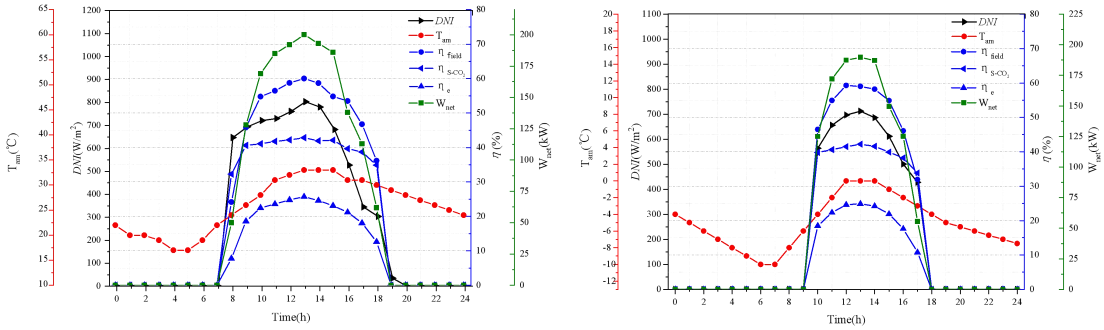

(a) Spring equinox **(b) Autumn equinox**

Fig. 8: Variation law of thermal performance of the system on typical day

Tab. 2: Cycle operation parameters under different loads

	100% load			75% load			50% load		
	T /℃	P /MPa	m /kg·s-1	T /℃	P /MPa	m /kg·s-1	T /℃	P /MPa	m /kg·s-1
Inlet of compressor	32	7.6	1.732	32	7.6	1.475	32	7.6	1.183
Outlet of compressor	74	20	1.732	68	17.6	1.475	61	15.1	1.183
Inlet of HX	385	20	1.732	402	17.6	1.475	423	15.1	1.183
Inlet of turbine	600	20	1.732	600	17.6	1.475	600	15.1	1.183
Outlet of turbine	479	7.6	1.732	495	7.6	1.475	514	7.6	1.183
Inlet of cooler	79	7.6	1.732	73	7.6	1.475	66	7.6	1.183
Cycle efficiency	42.83%			41.52%			38.75%		

4. Control Research

The running state of the whole system is initially designed as nine modes as shown in Fig. 9, and the program is carried out on TRNSYS simulation platform for each kind of running mode, which lays the foundation for the realization of control logic.

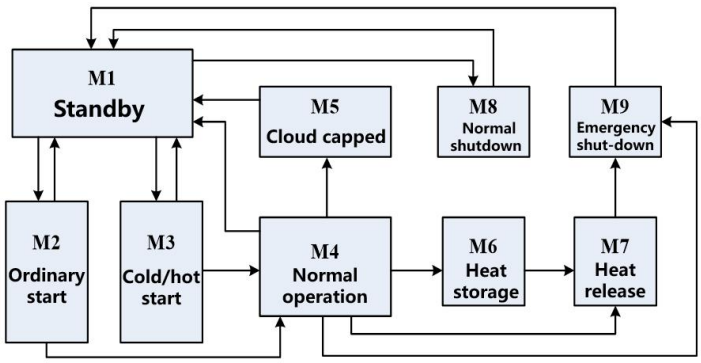

Fig. 9: sCO_2-CSP system operation mode

Different control strategies were to be used to study the operation of the system.

As shown in Fig. 10 (a), the conventional control strategy is fixed inventory control. Fixed carbon dioxide specific charge in the cycle provided sufficient performance on the design conditions. The “master” controller (PI1) decides the set-point for loop inventory to achieve the Turbine inlet temperature set-point. The “slave” controller (PI2) manipulates the carbon dioxide withdrawal /addition flowrate to track the loop inventory set-point proposed by the PI1.

As shown in Fig. 10 (b), one advanced control strategy is extremum-seeking control. Unlike the fixed inventory controller, in the extremum-seeking control approach, the particle/CO2 inventory can vary with time and the plant input is the inventory rate of change ($\dot{\theta}$). A sinusoidal dither is applied to the plant input to provide persistency of excitation in the gradient estimates at the output of the high pass filter. Inventory addition and removal is conducted at the compressor inlet to minimize any involved parasitic power losses. The proposed cost function (J) needs to incorporate the net power as well as the operating constraints on turbine inlet temperature and pressure. These operating constraints are considered through the introduction of slack variables. By changing the sign of the cost function and the high-pass filter, the extremum-seeker may be equally posed as a maximum or minimum seeking scheme.

The nonlinear slack variable operator is defined as:

$$\Gamma(x,y)=\begin{cases} 0 & if\ a<b \\ a-b & if\ a<b \end{cases} \quad \text{(eq.28)}$$

The cost function being proposed as:

$$J = P_{net} - \alpha\,\Gamma\left(T_{t,in}, T_{\max imun}\right) - \beta\,\Gamma\left(p_{t,in}, p_{\max imum}\right) \quad \text{(eq.29)}$$

Where α and β represent Slack variable weights, $T_{t,in}$ and $p_{t,in}$ represent inlet temperature and pressure of turbine.

As shown in Fig. 10 (c), the other advanced control strategy is differential evolution control. The basic idea of the control strategy from the initial turbine inlet temperature set point, use the net output power populations from different system randomly selected from the difference between the two individuals and vector as the third source of random variation, the individual will be poor after vector weighted sum according to certain rules and the third individual variation individuals, this operation is called mutation. Then, the variation individuals are mixed with the pre-determined system net output power target individuals to generate test individuals, a process called crossover. If the fitness value of the test individual is better than that of the target individual, the test individual will replace the target individual in the next generation; otherwise, the target individual will still be preserved. This operation is called selection. In the evolution process of each generation, each individual vector is used as the target individual once. The algorithm keeps good individuals and weeds out poor individuals through continuous iterative calculation to guide the search process to approach the global optimal solution.

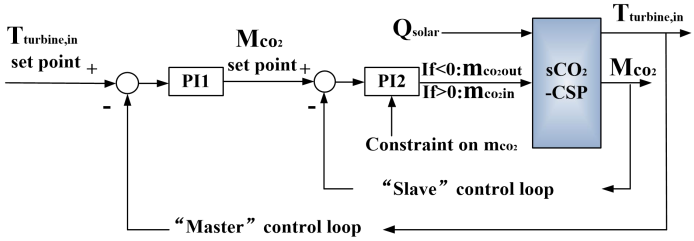

(a) Conventional fixed inventory control

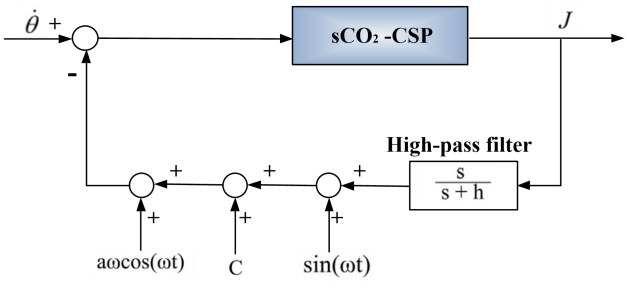

(b) Extremum-seeking control

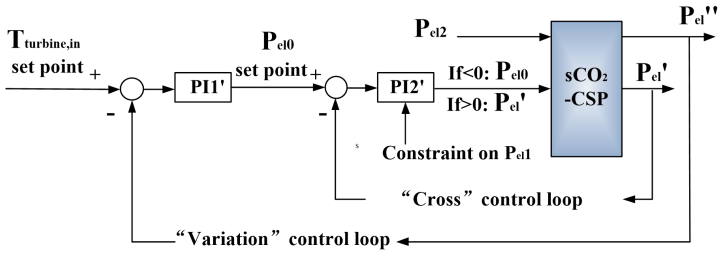

(c) Differential evolution control

Fig. 10: Different control strategies

Compared with the conventional fixed inventory control mode in the typical day with same number hours' heat storage. As shown in Fig. 11 (a), on the summer solstice, net solar power drops are small and unstable, the electricity production powered by extremum-seeking control is 1649.3kW, improved by 2.06%; the electricity production powered by differential evolution control is 1650.5kW, improved by 2.13%. As shown in Fig. 11 (b), on the winter solstice, net solar power drops significantly and permanently, the electricity production powered by extremum-seeking control is 1210.4kW, improved by 1.61%; the electricity production powered by differential evolution control is 1211.3kW, improved by 1.69%. However, when the DNI exceeds 600W/m^2, extremum-seeking control shows greater advantage compared with differential evolution control.

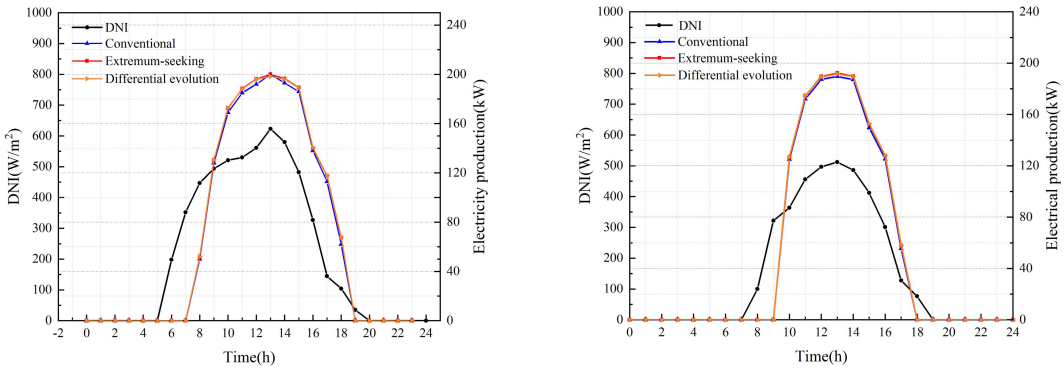

(a) Summer solstice **(b) Winter solstice**

Fig. 11: Electricity production under different control strategies on typical days

5. Conclusion

In this study, the basic thermodynamic properties of the supercritical carbon dioxide solar thermal power system were analyzed, the key parameters of the system were optimized and the dynamic simulation was carried out. Particle size is 0.5mm, simultaneously guarantee efficiency of receiver and coefficient of heat transfer of heat exchanger; Pressure ratio is 2.6, simultaneously guarantee specific work and cycle efficiency; Turbine inlet temperature is 650-700℃, simultaneously guarantee cycle efficiency and power generation efficiency; Compressor inlet temperature is 33℃, cycle thermal efficiency is the highest.

Based on dynamic simulation, different control strategies are studied, which has certain guiding significance for the efficient operation of the experiment. By comparing simulation results of different control strategies, extremum-seeking control of the system can be increased by 2.06%, differential evolution control of the system can be increased by 2.13%. However, when the DNI exceeds 600W/m^2, extremum-seeking control shows greater advantage compared with differential evolution control.

Work in progress also includes multi-condition experiment, multi-mode Control and multi-angle analysis. Related study aims to provide specific basic scientific research and route guidance for clean energy.

Clean energy innovation is critical to achieving net zero emissions and mitigating climate change. The energy sector can only achieve net zero emissions if there is a strong global push for clean energy innovation. There is a disconnect between climate targets set by governments and companies and efforts to develop better, lower-cost technologies. While tremendous advances in technologies such as solar have been witnessed, further changes are

needed in the pace of innovation and the scale of deployment of new technologies. Policy suggestions for promoting clean energy technology innovation are as follows:

- Determine innovation priority, track and adjust innovation progress. Review selected projects that require a mix of technologies that require public support to ensure that technological innovations are rigorous, collective, flexible, and consistent with local strengths.
- Promoting public research and development and market-led indigenous innovation. Scale up funding for different technologies using a range of tools, from public research and development to market incentives.
- Solve the problems in the clean energy innovation value chain. Look at the big picture and ensure that all components of the key value chain are advancing evenly towards the next market application and one exit effect.
- Build and enable infrastructure. Mobilize private financing to help companies cross the "valley of death" by co-sharing networks to enhance the investment risk of commercial scale demonstrations.
- Strive for regional innovation success on a global scale. Collaborate and share best practices, experiences and resources through existing multilateral platforms to address pressing global technological challenges.

Further in-depth research will be conducted on this new energy technology to promote the energy revolution, mitigate climate change, and make contributions to international climate governance and zero-carbon development.

6. Acknowledgments

The authors would like to thank the research grant support from the National Key Research and Development Project of China (No.2018YFB1501005).

7. References

Al-Sulaiman F.A., Atif M., 2015. Performance comparison of different supercritical carbon dioxide Brayton cycles integrated with a solar power tower. Energy. 82, 61-71.

Albrecht K J, Ho C K, 2018. High-temperature Flow Testing and Heat Transfer for a Moving Packed-Bed Particle/sCO_2 Heat Exchanger. AIP Conference Proceedings. 20-33.

Borodulya V A et al., 1991. Heat-transfer between a Surface and a Fluidized-bed - Consideration of Pressure and Temperature Effects. International Journal of Heat and Mass Transfer. 34, 47-53.

Cheang V.T., Hedderwick R.A., McGregor C., 2015. Benchmarking supercritical carbon dioxide cycles against steam Rankine cycles for concentrated solar power. Solar Energy. 113, 199-211.

Chen Y, Chao Q, 2021. Carbon peak and Carbon Neutral, People's Daily Press, Beijing.

Conboy T. et al., 2012. Performance Characteristics of an Operating Supercritical CO_2 Brayton Cycle. Journal of Eng. for Gas Turbines and Power. 134.

Daabo A.M., Ahmad A., Mahmoud S., Al-Dadah R.K., 2017. Parametric analysis of small scale cavity receiver with optimum shape for solar powered closed Brayton cycle applications. Appl. Therm. Eng. 122, 626–641.

Gnielinski V, 1976. New equations for heat and mass transfer in turbulent pipe and channel flow. Int Chem Eng. 16, 359-368.

He Y, Qiu Y, Wang K, 2000. Perspective of Concentrating Solar Power. Energy. 117-373.

Minh Tri Luu et al., 2018. Advanced control strategies for dynamic operation of a solar-assisted recompression supercritical CO_2 Brayton power cycle. Appl. Therm. Eng. 136, 682-700.

Nie F, Yu Y, Bai F, Wang Z, 2020. Experimental and numerical investigation on thermal performance of a quartz tube solid particle solar receiver. Solar Energy. 207, 1055-1069.

Singh R, Miller SA, Rowlands AS, Jacobs PA, 2013. Dynamic characteristics of a direct-heated supercritical carbon-dioxide brayton cycle in a solar-thermal power plant. Energy. 50, 194-204.

Wang Z, 2019. Design of Solar Thermal Power Plants, Chemical Industry Press, Beijing.

Wright S A, Conboy T M, Parma E J, 2011. Summary of the Sandia Supercritical CO_2 Development Program. Chinese Journal of Chemistry. 21, 1562-1564.